V European Conference on Computational Fluid Dynamics
ECCOMAS CFD 2010
J. C. F. Pereira and A. Sequeira (Eds)
Lisbon, Portugal,14-17 June 2010

# DIRECT NUMERICAL SIMULATION (DNS) OF TURBULENT FLOW OVER WAVY SURFACES

**Bojan Ničeno*** **and Simon Kuhn†**

*Paul Scherrer Institute,
5232 Villigen, Switzerland
e-mail: bojan.niceno@psi.ch
†Massachusetts Institute of Technology
Cambridge, USA

**Key words:** DNS, immersed boundary method (IBM), wavy walls

**Abstract.** *The present study adresses the turbulent flow over a wavy surface by direct numerical simulation (DNS). Compared to classical channel flow the wavy surface structure adds a degree of complexity to the flow by inducing streamline curvature, flow separation and flow reattachment, thus leading to flow situations which are often present in relevant technical and geophysical applications. The governing equations are discretized with a second order finite volume method on Cartesian, structured, staggered grids, and are integrated in time using the semi-implicit projection method. The wavy surface is represented with a variant of the immersed boundary method (IBM). The solution of the discretized system of linear equations is accelerated with an algebraic multigrid procedure. The simulations were performed on the Cray XT5 computer and scale well up to 128 processors. The flow over the wavy surface is particularly challenging for the IBM since the cells are cut at different angles in the regions where the most interesting phenomena like separation and reattachment takes place. In the present work, particular attention was payed on the size of the computational domain, ensuring it does not hinder the natural development of coherent structures in the considered flow. The results of the simulations compare favorably with particle image velocimetry (PIV) measurements, showing the IBM is an interesting candidate for simulating flows over wavy surfaces.*

## 1 INTRODUCTION

Technical and geophysical relevant flows are characterized by high Reynolds numbers and complex boundaries. The turbulent flow over these rough or structured surfaces is associated with increased transport of species (heat or mass) and momentum. Differently shaped wavy walls as boundaries of the flow resemble the wall complexity in a well–defined manner and therefore serve as test cases for the study of wall influence on turbulence. We investigate the turbulent flow between a flat top and a wavy bottom wall with a direct numerical simulation (DNS). The surface geometry is represented with an immersed boundary method (IBM) and we address the applicability of this technique to flows over complex surfaces.

The flow over a train of solid waves is connected to a developing shear layer, formed by the separation of the flow shortly after the wave crest, which extends over the whole wavelength[1]. For smooth walls flow-oriented vortical eddies have been associated with large Reynolds stresses and with the production of turbulence in the viscous region close to the wall[2]. Earlier experimental studies[3–6] investigated the structure and dynamics of turbulent motions in the outer part of the wall shear layer in a developed turbulent flow over waves and identified flow–oriented large–scale structures.

The forced convective flow over a wavy wall in fully devolved turbulent flow regimes has been extensively studied in literature. In a DNS by Cherukat et al.[1] the characteristics of the developing shear layer above the recirculation zone formed after the wave crest of a wavy wall with an amplitude–to–wavelength ratio of $\alpha = 0.05$ at a Reynolds number of 3460 (defined with the bulk velocity and the half channel height) was addressed. Large eddy simulations (LES) of forced convective wavy boundary flow were performed by Henn and Sykes[7], and Tseng and Ferziger[8]. In their extensive study Henn and Sykes focused on the effects of different wave slopes ranging from 0 to 0.628 on turbulence at $5720 \leq \mathrm{Re} \leq 20060$, where the wave slope is defined as $ak$, with the wavenumber $k = 2\pi/\Lambda_w$. They identified a scaling between the slope of small–amplitude waves and the velocity fluctuations, which is linear for the streamwise and vertical velocity components, but squared for the lateral. This is caused by the presence of coherent structures located at the upstream side of the wave. Tseng and Ferziger concentrated on these coherent structures for a wavy wall of $\alpha = 0.1$ at $\mathrm{Re} = 2400$, and illustrated the vortex formation and transport of Grtler vortices induced by the local wall curvature.

In the present study we perform a DNS of the turbulent flow over a wavy wall of $\alpha = 0.1$ at a Reynolds number of $\mathrm{Re} = 11200$. We compare the results of the simulations with particle image velocimetry (PIV) measurements to address the applicability of the implemented IBM. Furthermore we focus on the influence of the spanwise extend of the computational domain on the resulting flow structures.

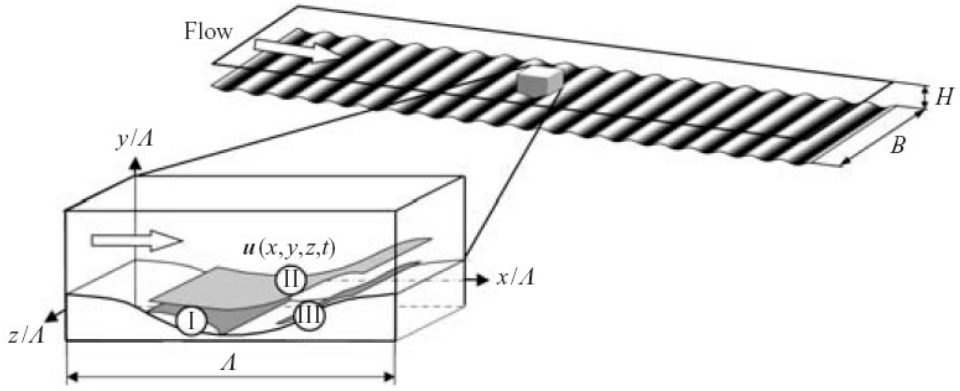


Figure 1: Coordinate system and schematic of (I) the separation region, and the regions (II) of maximum positive and (III) maximum negative Reynolds shear stress for a flow situation with separation.

## 2 FLOW DESCRIPTION AND EXPERIMENTS

We consider the flow over a solid wavy bottom wall characterized by the Reynolds number

$$\mathrm{Re}_h = \frac{U_B \cdot h}{\nu}, \tag{1}$$

where $\nu$ denotes the kinematic viscosity, and $h$ is the half-height of the channel. The bulk velocity $U_B$ is defined as

$$U_B = \frac{1}{(2h - y_w)} \int_{y_w}^{2h} U(x_\xi, y) dy, \tag{2}$$

calculated at an arbitrary $x$-location, $x_\xi$. The wall profile, characterized by the amplitude $2a$ and the wavelength $\Lambda$, is described by

$$y_w(x) = a \cdot \cos(2\pi x/\Lambda). \tag{3}$$

Figure 1 shows the coordinate system and schematically illustrates characteristic regions of the flow field in the vicinity of the wavy surface. The coordinate $x$ is directed parallel to the mean flow, $y$ is perpendicular to the top wall, and $z$ is the spanwise coordinate direction. The corresponding velocity components are denoted as $u$, $v$, and $w$. Characteristic regions of a flow over waves with separation, reported by Cherukat et al.[1], and Henn and Sykes[7], are the separation region (I), and the regions of maximum positive (II) and maximum negative (III) Reynolds shear stress $-\varrho\overline{u'v'}$. The geometry of the wavy wall is determined by the ratio of the amplitude, $2a$, to the wavelength, $\Lambda$,

$$\alpha = \frac{2a}{\Lambda}. \tag{4}$$

If the amplitude–to–wavelength ratio $\alpha$ is large enough, flow separation can be observed[9].

Measurements were carried out in a water channel facility designed for turbulence measurements with light sheet techniques at Reynolds numbers up to 21000, defined with the bulk velocity $U_B$ and the half channel height $h$. The full height of the channel, $H$, is 30 mm, and its aspect ratio (width $B$ to height $H$) is 12:1. The incorporated wavy wall has a wavelength of 30 mm and an amplitude of 3 mm, which results in $\alpha = 0.1$. Optical access is provided at four streamwise positions through viewing ports, positioned at both sidewalls and at the flat top wall. Measurements are performed for a hydrodynamically developed turbulent flow after the 50th wave crest. Digital particle image velocimetry (PIV) is performed to examine the spatial variation of the streamwise, spanwise and wall–normal velocity components[10,11]. Measurements are performed at a Reynolds number of 11200, and we consider an ensemble of 1000 consecutive images pairs acquired at a frame rate of 4 Hz. A flashlamp–pumped dual Nd:YAG-laser provides the pulse light source, a 10-bit CCD camera with a pixel-resolution of $1280 \times 1024$ pixels$^2$ is used for the velocity measurements. The uncertainty of the PIV measurements resulting from the experimental setup, image acquisition and image processing is estimated to be in the order of 1%[12].

## 3 NUMERICAL DETAILS

In the presented work we solve the equations describing incompressible flows with constant fluid properties. For time discretization the governing equations are integrated in time using a semi-implicit projection method[13]. Viscous terms in momentum equations are discretized with a Crank-Nicolson scheme for stability, wheres the advective terms are discretized with the Adams-Bashforth scheme for simplicity. For spatial discretization the governing equations are discretized on a three-dimensional Cartesian grid by balancing fluxes of transported variables over the cell faces with inertial and forcing terms. Momentum equations are discretized on a staggered grid for numerical robustness. Figure 2 depicts the logical coordinates and the cell face dimensions in the structured Cartesian grid. Logical indices represent cell face values if they contain the term $\delta$, or cell-centered values if they contain the term $2\delta$. The final form of the discretized equation for a general variable $\phi$ reads:

$$\begin{aligned} a_C^{i,j,k}\phi^{i,j,k} + a_W^{i,j,k}\phi^{i-2\delta,j,k} + a_E^{i,j,k}\phi^{i+2\delta,j,k} \\ + a_S^{i,j,k}\phi^{i,j-2\delta,k} + a_N^{i,j,k}\phi^{i,j+2\delta,k} \\ + a_B^{i,j,k}\phi^{i,j,k-2\delta} + a_T^{i,j,k}\phi^{i,j,k+2\delta} &= b^{i,j,k}, \end{aligned} \tag{5}$$

where $a_C^{i,j,k}$ is the diagonal and coefficients $a_W^{i,j,k}$ to $a_T^{i,j,k}$ the off-diagonal entries in the system matrix for the variable $\phi^{i,j,k}$. The source term is represented by $b^{i,j,k}$.

The immersed body is represented in our approach by its triangulated surface. For the sake of compatibility with computer aided design (CAD) programs, we import the immersed body from a file in stereo-lithographic (STL) format. STL files define triangulated surfaces by the coordinates of the triangle's vertices and normal surface vectors.

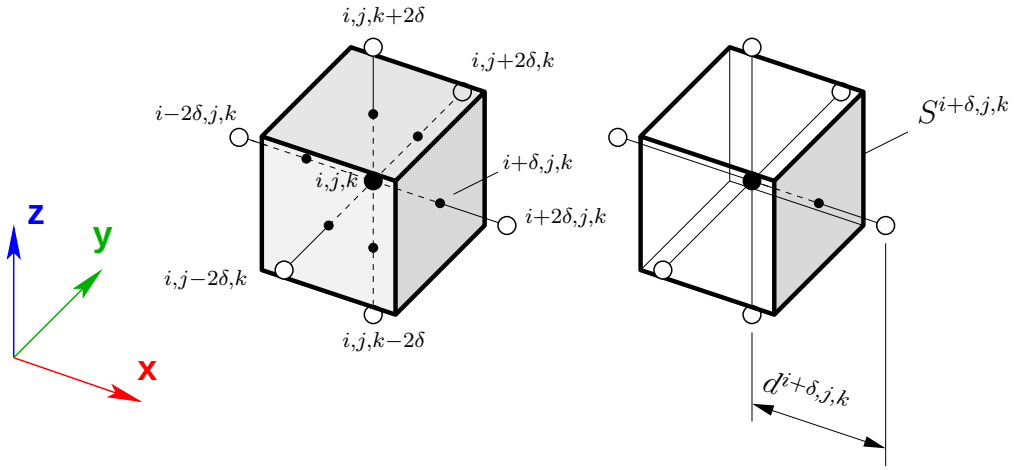


Figure 2: Logical coordinates (a) and cell face dimensions (b) in the structured Cartesian grid. Cell-centered values are denoted with indices containing $2\delta$, while the cell face values contain $\delta$. For example, the cell face between cells $i, j, k$ and $i + 2\delta, j, k$ is denoted by $i + \delta, j, k$.

These triangulated surfaces are used to cut the individual grid cells. Since we are using a staggered grid approach, we have four finite volume grids: one for the scalar variables and one each for the three velocity components. To cope with immersed boundaries, we cut all three grids separately as illustrated in Fig. 3.

Once the cells in all four grids are cut, they are classified into three sets:

- *Cut* cells, belonging to set C, are the cells which are intersected by the immersed boundary.
- *Fluid* cells, belonging to set F, are the cells whose center remains in the fluid part of the domain, no matter if they are cut or not.
- *Solid* cells, belonging to set S are all those which are not in set F, i.e. the cells who's center lies in the solid part of the domain.

According to this classification, a cell can belong to two sets simultaneously. As there are four cells in the staggered approach adopted, here there are also four sets of classifications into C, F and S. A sample domain, plotted in 2D for the sake of clarity, with sets C, F and S is shown in Fig. 4. Figure 4(a) shows a computational grid, with each cell center denoted with a black dot. The immersed body is represented by a shaded area. The cells whose cell center lies in fluid belong to set F, while the rest of the cells belongs to set S as illustrated in Fig. 4(b). The cells which are cut with the immersed body, also belong to set C.

Cuts performed on the computational cells change their geometrical properties, and closely associated with that the discretized system of equations (5). Geometrical quantities featured in Eq. (5) are the cell *volumes*, entering the system matrix through the

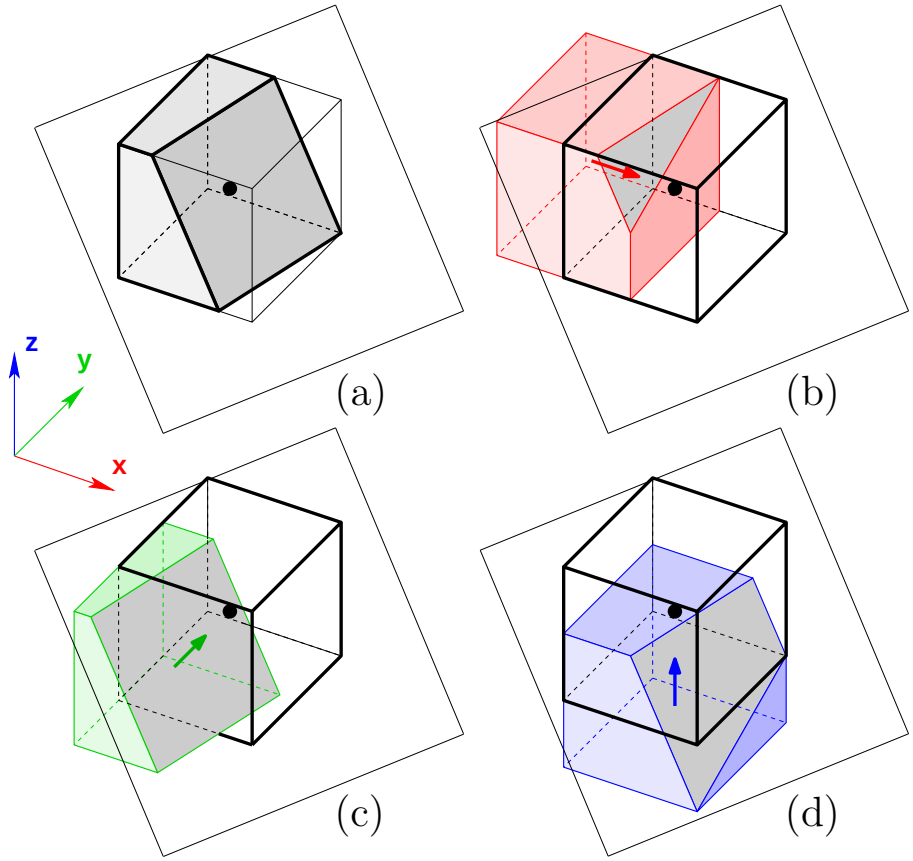


Figure 3: Each grid is cut separately: (a) scalar cell, (b), (c) and (d) momentum cells in $x$, $y$ and $z$ directions respectively.

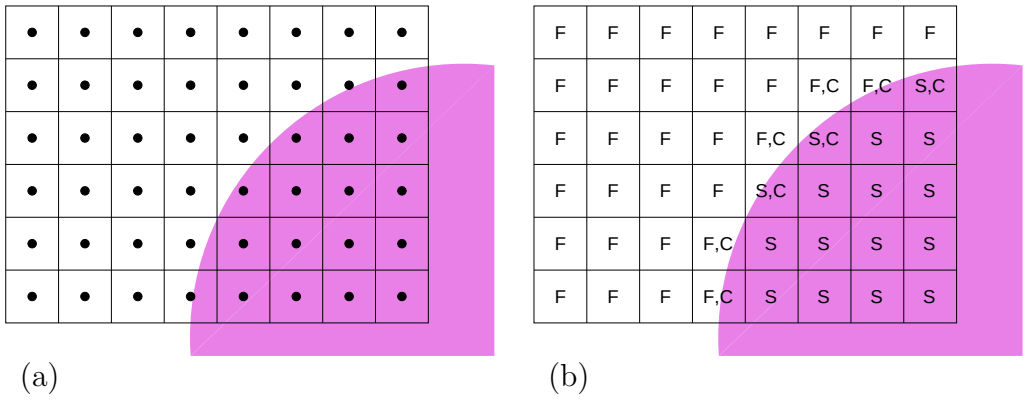


Figure 4: A sample computational domain with classified cells: (a) cell centers, (b) sets. The shaded area represents the immersed body.

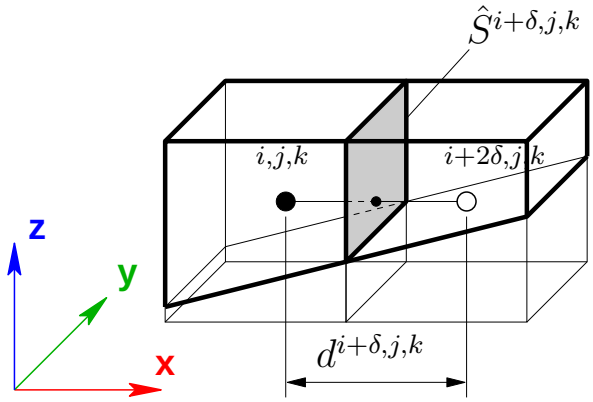


Figure 5: Both cells surrounding connection $i+\delta, j, k$ are cut, but their centers are in the fluid. The effective diffusive flux through the connection diminishes in proportion to the reduced face area.

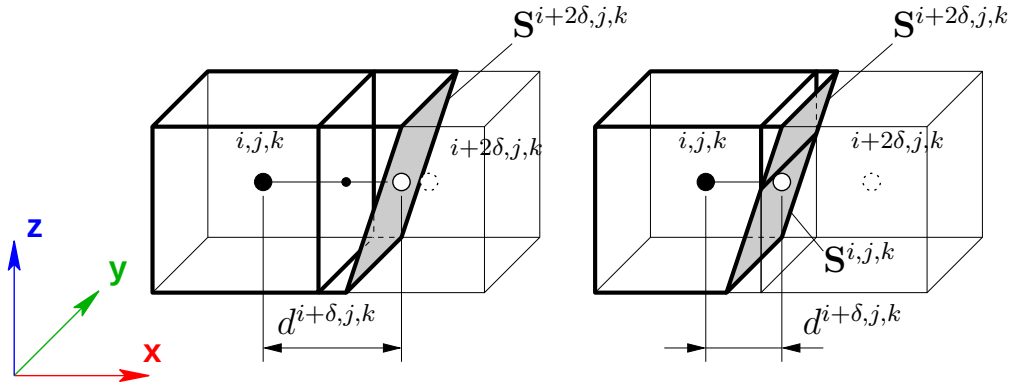


Figure 6: Cell face at $i+\delta, j, k$ is between the fluid cell $i, j, k$ and the solid cell $i+2\delta, j, k$.

inertial terms, the *distances* between cell centers, and the cell face *areas*. For the evaluation of the diffusion terms modified for the presence of the immersed body two different cases have to be considered. The first occurs if both cells surrounding the face for which the diffusive flux is estimated belong to fluid set (F). Such a situation, for the cell face $i+\delta, j, k$ is illustrated in Fig. 5. In such a case, the distance between the cells remains unchanged, but the cell face area between them changes, affecting the diffusive flux through the cell face, which needs to be accounted for in the equations solved. A different approach has to be taken if one cell, say $i+2\delta, j, k$ is in the solid. Two such situations are illustrated in Fig. 6. In such a case, the cell in the solid becomes effectively a boundary cell, and the distance between the cells decreases. That is accounted for by defining the ratio between the new and the old distances between the cells. The area is not corrected in this case. We assume that the gradient of the advected variable in $x$ direction is constant at the

face center $i+\delta, j, k$, so the area which plays a role in the diffusive flux is the projection of the slanted surface ($\mathbf{S}^{i+2\delta,j,k}$ in Fig. 6(a), or $\mathbf{S}^{i,j,k} + \mathbf{S}^{i+2\delta,j,k}$ in Fig. 6(b)), on the plane normal to $x$, which is just $S^{i+\delta,j,k}$ on the original grid.

## 4 RESULTS

In this section we compare the DNS results with PIV measurements. This is followed by a discussion of the influence of the spanwise domain width on the developing flow structures.

The simulations were performed for a wavy wall with $\alpha = 0.1$ ($\Lambda = 30$ mm) at a Reynolds number of $\mathrm{Re}_h = 11200$. To investigate the influence of the spanwise domain width three different geometries were used, where the spanwise width was (i) $1.0H$, (ii) $1.5H$, and (iii) $2.0H$ respectively. The cell size of the numerical mesh was $\Delta x = H/128$, $\Delta y = H/256$, and $\Delta z = H/128$ for all cases. This gives a total number of cells of (i) 4194304, (ii) 6291456 and (iii) 8388608, simulated on (i) 128, (ii) 192 and (iii) 256 processors respectivelly, thus keeping the number of cells per processor constant. Scaling was pretty good in this range and each simulation required 4 days (96 hours) of wall-clock time. For each simulation we performed 240000 time steps corresponding to 300 flow-through times. Statistics reported below was gather over the final 150 flow-throuh times.

### 4.1 Comparison to experimental data

To validate the numerical results vertical velocity profiles at different streamwise locations $x/H$ along the wavy surface are plotted, where $x/H = 0.00$ and $x/H = 1.00$ denote the wave crest, $x/H = 0.50$ the wave trough, and $x/H = 0.25$ and $x/H = 0.75$ the inflection point of the wall profile. Figure 7 depicts the comparison of the mean streamwise and vertical velocity profiles for $\mathrm{Re}_h = 11200$. A good agreement between experiments and simulations is obtained for the mean streamwise velocity component at all locations (Fig. 7(a)). The influence of the wavy surface is expressed by the asymmetric shape of the flow profile. The maximum value of the mean streamwise velocity component is found for a wall-normal distance of $y/H = 0.7$. Negative values of the velocity at the streamwise positions $x/H = 0.25$ and $x/H = 0.50$ indicate flow separation and a recirculation zone at the downstream side of the wave. The vertical velocity component profiles show a similar good agreement with an exception at the positions $x/H = 0.50$ and $x/H = 0.75$, where the DNS profiles show higher values in comparison with the PIV data (Fig. 7(b)). This region of the flow is primarily affected by the recirculative motion caused by the separation after the wave crest and therefore the $v$–component of the velocity is most susceptible to measurement uncertainties.

Figure 8 depicts the comparison of the streamwise and vertical normal stress profiles for $\mathrm{Re}_h = 11200$. Also this comparison reveals a good agreement between the experiment and the simulation for the turbulent statistics. Therefore we conclude that the DNS approach with the IBM method performs well in the prediction of turbulent flow over a wavy wall.

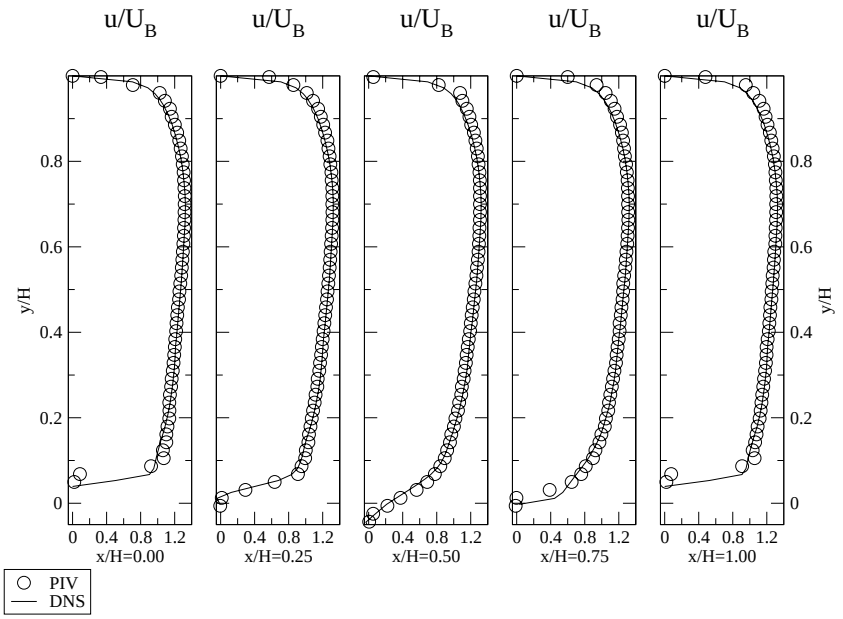


(a) Mean streamwise velocity

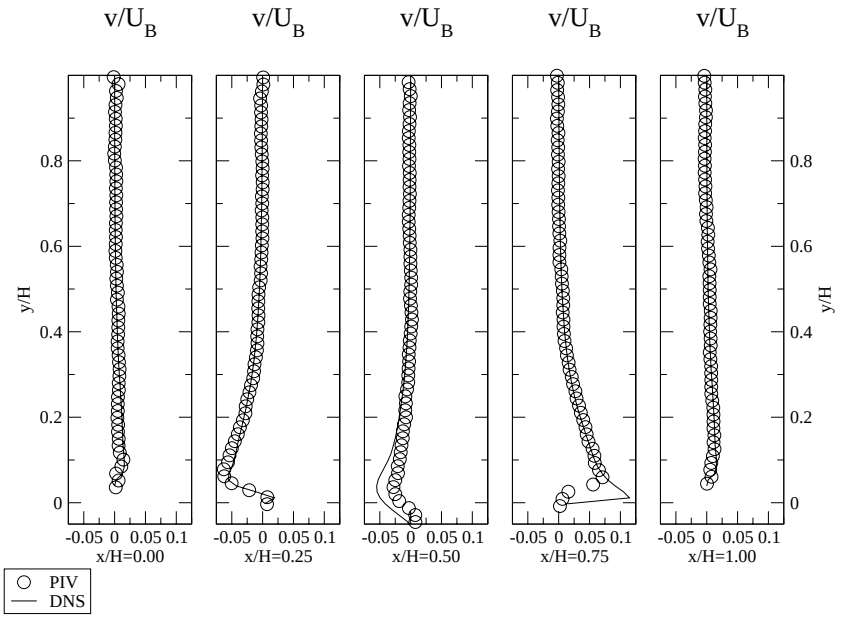


(b) Mean vertical velocity

Figure 7: Comparison of the mean velocity profiles between particle image velocimetry data and direct numerical simulation of turbulent flow over a wavy wall, $\mathrm{Re}_h = 11200$.

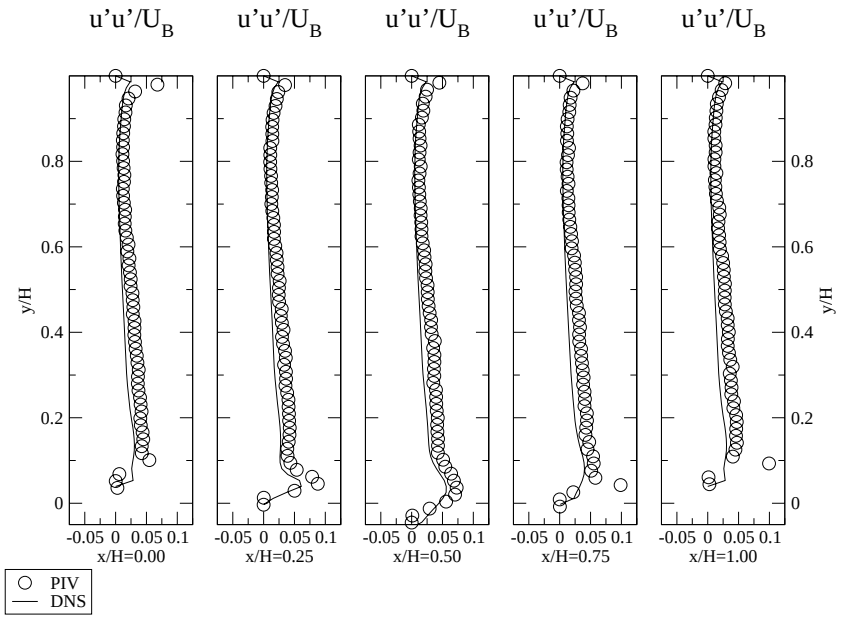


(a) Streamwise normal stress

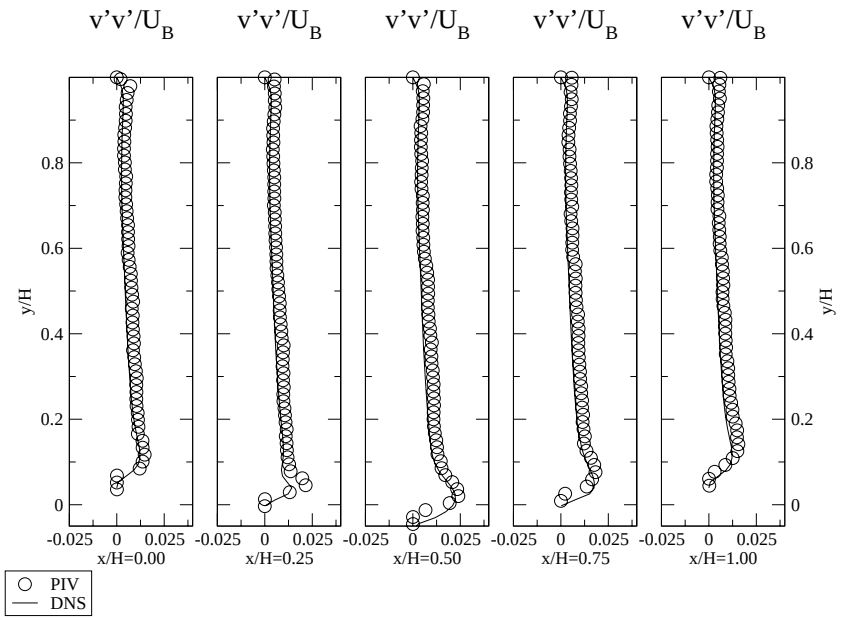


(b) Vertical normal stress

Figure 8: Comparison of the normal stress profiles between particle image velocimetry data and direct numerical simulation of turbulent flow over a wavy wall, $\mathrm{Re}_h = 11200$.

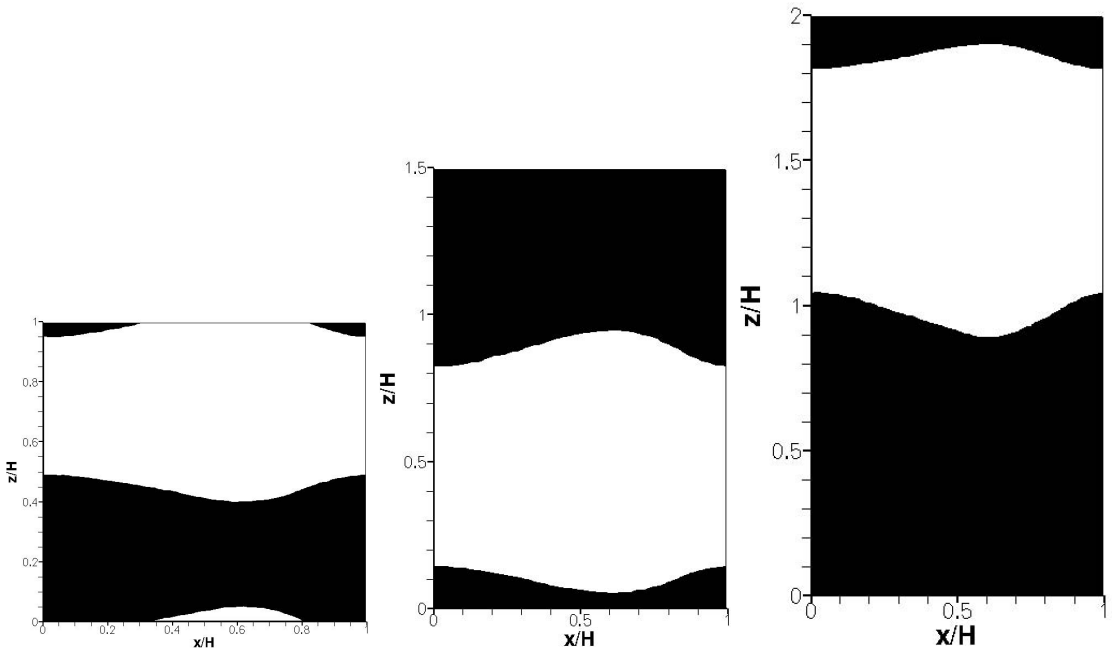


(a) Width $1.0H$ (b) Width $1.5H$ (c) Width $2.0H$

Figure 9: Contours of the streamwise velocity in the plane $y/H = 0.2$ for $\mathrm{Re}_h = 11200$. The white area corresponds to $u < U_B$, the black area to $u > U_B$. Flow is from left to right.

### 4.2 Influence of domain width

Experimental studies showed the existence of longitudinal flow structures in the turbulent flow over solid waves[6]. For the wavy wall with $\alpha = 0.1$ ($\Lambda = 30$ mm) these coherent structures have a spanwise spacing of $1.5H$. This spacing of the longitudinal structures can be identified by plotting contours of the streamwise velocity in a plane parallel to the mean flow at $y/H = 0.20$. Figure 9 shows that these flow structures can be identified as fluid streaks traveling faster (black area) or slower (white area) compared to the adjusted bulk velocity $U_B$. Their spanwise spacing is given by the distance between two fluid streaks traveling with faster or lower velocity compared to the bulk velocity. To identify this spacing we plot the profiles of the streamwise averaged velocity component $u/U_B$ in Fig. 10. The influence of the size of the computational domain on the spanwise distance of the flow structures is evident. For a spanwise domain width of $1.0H$ and $1.5H$ the spacing of the flow structures is also found to be $1.0H$ and $1.5H$ respectively. For a domain width of $2.0H$ the observed spanwise distance is $1.9H$. This result suggests that for the domain width of $2.0H$ the spacing of the coherent structures is no longer or only weakly linked to the size of the computational domain and the natural development of coherent structures is not hindered. However, this spanwise distance of $1.9H$ differs from the available experimental results which suggest a spacing of $1.5H$. This issue needs

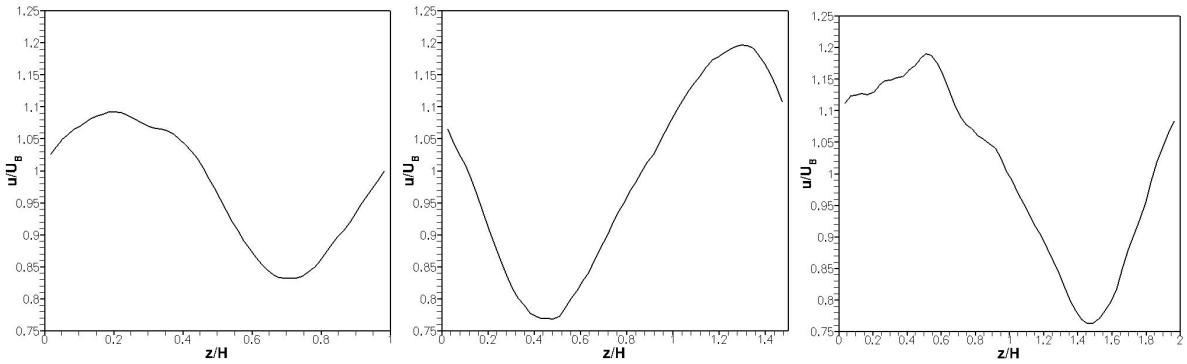


(a) Width $1.0H$ (b) Width $1.5H$ (c) Width $2.0H$

Figure 10: Profiles of the streamwise averaged velocity component $u/U_B$ in the plane $y/H = 0.2$ for $\mathrm{Re}_h = 11200$.

further clarification by applying analytical tools like the proper orthogonal decomposition (POD) to the DNS data.

## 5 CONCLUSIONS

This paper presents the application of DNS with an implementation of the Immersed Boundary Method (IBM) to the turbulent flow over solid waves. The governing equations are first discretized using the Cartesian, staggered, finite volume method. The resulting systems of linear equations are then corrected for the presence of the immersed body by recomputing individual entries where needed. The simple structure of the Cartesian grid facilitated usage of an efficient algebraic multigrid solver, but special care had to be taken with the modifications performed on the discretized system of equations not to hinder its convergence properties.

The method has been verified by computing the flow over solid waves with $\alpha = 0.1$ ($\Lambda = 30$ mm at a Reynolds number of $\mathrm{Re}_h = 11200$. The flow over the wavy surface is particularly challenging for the IBM since the cells are cut at different angles in the regions where the most interesting phenomena like separation and reattachment take place. The comparison with PIV data from an identical experimental setup reveals a good agreement for the mean velocity components and the normal stresses. Thus the DNS approach with the IBM method performs well in the prediction of turbulent flow over a wavy wall.

The influence of the width of the computational domain on the spanwise spacing of longitudinal flow structures developing over the train of waves was addressed by plotting contours of the streamwise velocity in a plane parallel to the mean flow at $y/H = 0.20$. The longitudinal flow structures were identified as fluid streaks traveling faster or slower than the adjusted bulk velocity $U_B$. For a spanwise domain width of $1.0H$ and $1.5H$ the spacing of the flow structures is also found to be $1.0H$ and $1.5H$ respectively. For a domain width of $2.0H$ their spanwise spacing seems to be independent of the domain size.

The observed value of $1.9H$ is larger than the experimental result of $1.5H$. Therefore further validation in this regard is needed.

## References


[1] P. Cherukat, Y. Na, T. J. Hanratty and J. B. McLaughlin, Direct numerical simulation of a fully developed turbulent flow over a wavy wall, *Theor. Comp. Fluid Dyn.*, **11**(2), 109–134 (1998).

[2] J. W. Brooke and T. J. Hanratty, Origin of turbulence–producing eddies in a channel flow, *Phys. Fluids*, **A 5**, 1011–1022 (1993).

[3] A. Günther and P. Rudolf von Rohr, Ph., Large scale structures in a developed flow over a wavy wall, *J. Fluid Mech.*, **478**, 257–285 (2003).

[4] N. Kruse, A. Günther and P. Rudolf von Rohr, Dynamics of large–scale structures in a turbulent flow over a wavy wall, *J. Fluid Mech.*, **485**, 87–96 (2003).

[5] N. Kruse, S. Kuhn and P. Rudolf von Rohr, Wavy wall effects on turbulence production and large–scale modes, *J. Turbulence*, **7(31)**, 1–28 (2006).

[6] S. Kuhn, C. Wagner and P. Rudolf von Rohr, Influence of wavy surfaces on coherent structures in a turbulent flow, *Exp. Fluids*, **43**, 251–259 (2007).

[7] D. S. Henn and R. I. Sykes, Large eddy simulation of flow over wavy surfaces, *J. Fluid Mech.*, **382**, 75–112 (1999).

[8] Y.-H. Tseng and J. H. Ferziger, Large-eddy simulation of turbulent wavy boundary flow – illustration of vortex dynamics, *J. Turbulence*, **5**, 1–23 (2004).

[9] J. Buckles, T. J. Hanratty and R. J. Adrian, Turbulent flow over large-amplitude wavy surfaces, *J. Fluid Mech.*, **140**, 27–44 (1984).

[10] R. J. Adrian, Particle-imaging techniques for experimental fluid mechanics, *Ann. Rev. Fluid Mech.*, **23**, 261–304 (1991).

[11] M. Raffel, C. Willert and J. Kompenhans, J., Particle image velocimetry. A practical guide, *Springer*, 1998.

[12] S. Kuhn and P. Rudolf von Rohr, Experimental study of heat flux in mixed convective flow over solid waves, *Exp. Fluids*, **44**, 973–984 (2008).

[13] A. J. Chorin , Numerical solution method for the Navier-Stokes equations, *Math. Computat.*, **22**, 745–762 (1968).